Hemisphere-Dependent Impacts of ENSO and Atmospheric Eddies on Hadley Circulation

MAHDI HASAN,[a] SARAH M. LARSON,[a] KAY MCMONIGAL,[a,b] WALTER A. ROBINSON,[a] AND ANANTHA AIYYER[a]

[a] *Department of Marine, Earth, and Atmospheric Sciences, North Carolina State University, Raleigh, North Carolina*
[b] *College of Fisheries and Ocean Sciences, University of Alaska Fairbanks, Fairbanks, Alaska*

(Manuscript received 17 February 2024, in final form 19 July 2024, accepted 16 September 2024)

ABSTRACT: The variability of the Hadley circulation strength (HCS), crucial to tropical climate variability, is attributed to both oceanic and atmospheric forcings. El Niño–Southern Oscillation (ENSO) and variations in the extratropical upper-tropospheric eddies are the known drivers of the interannual HCS variability. However, the relative contributions of these oceanic and atmospheric forcings to the hemispheric HCS variability are not well understood. In particular, how much anomalous wind stress–driven ocean dynamics, including ENSO, impact HCS variability remains an open question. To address these gaps, we investigate the drivers of the interannual HCS variability using global coupled model experiments that include or exclude anomalous wind stress–driven ocean circulation variability. We find that the anomalous wind stress–driven ocean circulation variability significantly amplifies HCS variability in the Southern Hemisphere (SH). ENSO is the leading modulator of the SH HCS variability, which offers the potential to improve the predictability of Hadley circulation (HC)–related hydrological consequences. On the other hand, the Northern Hemisphere (NH) HCS variability is predominantly influenced by the eddy-driven internal atmospheric variability with little role in ocean dynamics. We hypothesize that the large eddy variability in the NH and concentrated ENSO-associated heating and precipitation in the SH lead to the hemisphere-dependent differences in the interannual HCS variability.

KEYWORDS: ENSO; Hadley circulation; General circulation models; Internal variability; Oceanic variability

1. Introduction

The Hadley circulation (HC) is a fundamental component of the atmospheric general circulation. The HC influences the global weather and climate by redistributing heat, moisture, and energy from the tropics to higher latitudes. On a large scale, the HC is often defined by the zonal-mean meridional atmospheric circulation (Vallis 2017), characterized by upward motion related to moist convection in the tropics and subsidence in the subtropics. Hence, the variability of the HC is fundamentally connected to the variability of the wet and arid climates that characterize the tropical and subtropical regions (Feng and Fu 2013; Scheff and Frierson 2012; Schmidt and Grise 2017). A change in the pattern and intensity of the HC directly influences the hydrological cycles in these regions.

Many authors have argued that global climate change has affected the strength of the HC (Quan et al. 2004; Mitas and Clement 2005, 2006; Stachnik and Schumacher 2011; Nguyen et al. 2013; Hu et al. 2018; Zaplotnik et al. 2022). Analysis of most observational and reanalysis datasets show an increase in the Hadley circulation strength (HCS) in the Northern and Southern Hemispheres over the past few decades (Tanaka et al. 2004; Mitas and Clement 2006; Stachnik and Schumacher 2011; Nguyen et al. 2013; Zaplotnik et al. 2022; Latif et al. 2023). Climate model simulations, however, show a weakening trend in the HCS over the same period, especially in the Northern Hemisphere (NH) (Held and Soden 2006; Vecchi and Soden 2007; Kang et al. 2013; Vallis et al. 2015; Chemke and Polvani 2019). Chemke and Polvani (2019) found that the contrasting trend between reanalysis products and climate models in the NH over the historical period is partly due to artifacts in the representation of the latent heat flux in reanalysis products, a bias previously discussed by Held and Soden (2006). Future climate projections suggest that the HCS will continue to change if the global temperature continues to rise in response to anthropogenic forcing (Vecchi and Soden 2007; Levine and Schneider 2011; Lau and Kim 2015; Chemke and Polvani 2018, 2019; Chemke 2021; D. Kim et al. 2022; Latif et al. 2023). Notably, there is a projected weakening of the NH HCS and no significant Southern Hemisphere (SH) HCS trend in future climate simulations (Vallis et al. 2015; Lau and Kim 2015; Hu et al. 2018; Xia et al. 2020; D. Kim et al. 2022), which differs from what has been observed over the historical period. Hence, there is a large uncertainty associated with the trend in the HCS.

The uncertainty in the future HCS can be attributed to factors that include, but are not limited to, the uncertainty in future emission scenarios, "noise" associated with the internal climate variability and differences in model numerical representations of physical processes (Deser et al. 2012; Shepherd 2014), such as model uncertainty in the cloud feedback (Deser et al. 2012; Shepherd 2014; Voigt and Shaw 2015; Ceppi and Shepherd 2017; H. Kim et al. 2022). Apart from known biases in the reanalysis products (Chemke and Polvani 2019), the discrepancy between the historical HCS trends in the models and reanalyses in both hemispheres can also be largely attributed to internal climate variability that can project onto the

Supplemental information related to this paper is available at the Journals Online website: https://doi.org/10.1175/JCLI-D-24-0112.s1.

Corresponding author: Mahdi Hasan, mhasan6@ncsu.edu

DOI: 10.1175/JCLI-D-24-0112.1

trend (Nguyen et al. 2013; Zaplotnik et al. 2022). Furthermore, future climate projections also exhibit a considerable spread in the HCS trend (Gastineau et al. 2008; Kang et al. 2013). Kang et al. (2013) mentioned that the uncertainty in the future HCS may be associated with uncertainty in the underlying sea surface temperature (SST) conditions. Our goal here is to identify the relative importance of different internal processes that drive HCS variability and potentially contribute to uncertainties in current and future HCS trends.

Interannual HCS variability has been linked to both oceanic and atmospheric forcings. In the atmosphere, upper-tropospheric eddies are known modulators of HC variability (Kim and Lee 2001; Walker and Schneider 2006; Caballero 2007; Zurita-Gotor and Álvarez-Zapatero 2018). Indeed, from the zonal-mean perspective, the upper-atmospheric momentum transport is connected to the HC mass flux through a first-order balance between meridional advection of absolute vorticity (or absolute angular momentum) and the divergence of eddy momentum fluxes (EMFs) such that

$$(f + \overline{\zeta})\overline{v} \approx S, \tag{1}$$

$$S = (a\cos^2\phi)^{-1}\partial_{\phi}(\overline{u'v'}\cos\phi), \tag{2}$$

where ζ is the relative vorticity; u and v are the zonal and meridional velocity components, respectively; f is the Coriolis parameter; ϕ is the latitude; a is Earth's radius; S is the eddy momentum flux divergence (EMFD); overbars represent the climatological zonal mean; and primes denote the deviation from the zonal mean. In the deep tropics, proximate to the intertropical convergence zone (ITCZ) and the rising branch of the HC, the absolute angular momentum of the upper-atmospheric diverging flow is approximately conserved (Schneider and Lindzen 1977; Held and Hou 1980), and S is small. Outside of that narrow zone, however, S is positive in the NH and negative in the SH such that the strength of the poleward flow (i.e., $\overline{v}$) varies in proportion to the divergence of the eddy momentum flux. The HC then no longer follows an angular momentum–conserving solution, and variations in HCS are then connected to variations in the eddy momentum flux. In fact, without eddy contributions, the HCS is weaker in axisymmetric models with symmetric thermal driving compared to eddy-permitting models (Kim and Lee 2001; Walker and Schneider 2005). Davis and Birner (2019) showed that the eddies allow the HC to transport more heat and momentum poleward. Caballero (2007) found that the extratropical eddies largely control the boreal winter HCS variability in the NH in reanalysis datasets. Using idealized GCMs, Walker and Schneider (2006) demonstrated that the HCS is directly related to the eddy momentum flux divergence and the extratropical climate is important for the tropical HC. Hence, eddies are an important source of interannual HCS variability with a larger imprint in the winter hemispheres with their strong eddy activity.

On the other hand, the oceanic driver that predominantly modulates the interannual HCS variability is associated with El Niño–Southern Oscillation (ENSO). Oort and Yienger (1996) found that the observed HCS is stronger during the warm phase of ENSO (i.e., El Niño) and weaker during the cold phase (i.e., La Niña) with a stronger correlation in the SH than in the NH. A consistent linear response of the HCS to ENSO phase was also demonstrated by Quan et al. (2004) using composite analysis from the National Center for Environmental Protection and the National Center for Atmospheric Research (NCEP–NCAR) reanalysis dataset. However, they found a secondary counterclockwise anomalous meridional circulation, contrary to the clockwise climatological meridional circulation in the NH subtropics (~15° to 30°N). This anomalous counterclockwise circulation may potentially result in a weaker HC response to ENSO in the NH than in the SH. Mechanistically, ENSO exerts a direct influence on the HC through diabatic heating in the tropical Pacific, and it impacts the extratropical circulation indirectly through changes in the transient eddy momentum fluxes (Seager et al. 2003, 2005; Robinson 2006). Ji et al. (2023) found that ENSO phases modulate the HCS by regulating the thermal forcing in the Indo-Pacific warm pool (IPWP) region. Using CMIP6 model simulations, Li et al. (2023) concluded that the models accurately representing ENSO exhibit a strong relation between the tropical meridional SST gradient and HC. During ENSO phases, tropical heating/cooling in the eastern and central equatorial Pacific creates a pronounced anomalous meridional SST gradient, which subsequently induces a stronger/weaker HC following nonlinear axisymmetric theory (Schneider 1977; Held and Hou 1980). According to the nonlinear axisymmetric theory, the HC is a thermally closed circulation with an angular momentum conserving upper-atmospheric poleward flow. For an anomalous positive meridional temperature gradient, the upper-atmospheric flow intensifies, thereby strengthening the circulation following the thermal wind balance.

Alternatively, it was argued in other studies that ENSO is negligible in driving interannual HCS variability (Tanaka et al. 2004; Mitas and Clement 2005; Chemke 2022; Zaplotnik et al. 2022). Chemke (2022) found that both the SH and NH HCS variability are weakly correlated with the Niño-3.4 index. Zaplotnik et al. (2022) found that the interannual HCS variability positively correlates with the Niño-3.4 index only in the SH, whereas the correlation is negative for the NH HCS. Similarly, Zhou et al. (2020) showed that the warming in the equatorial eastern Pacific (e.g., El Niño) acts to weaken the HCS in the NH but strengthens HCS in the SH. The discrepancy in the relationship between HCS and ENSO among previous studies may stem from several sources, including the varying definitions of HCS and its annual mean and the use of different data sources.

Even more broadly than ENSO itself, only a handful of studies have aimed to understand the role of ocean circulation in the HC (Clement 2006; Levine and Schneider 2011; Chemke and Polvani 2018; Chemke 2022). Using idealized model simulations, Levine and Schneider (2011) found that the coupling between wind stress and oceanic heat transport is important to obtain the observed mean HCS in climate models. Clement (2006) suggested that the variability of ocean heat transport plays a significant role in the seasonal variability of HCS by changing the location of the SST maxima and the corresponding convection. Chemke (2022) found that the oceanic heat flux convergence is primarily responsible for the large hemispheric

difference in HCS variability, with an opposite impact in the NH and SH.

The above studies that investigated the ocean circulation impact in the HC typically compare a fully coupled model with a dynamic ocean to a similar model but with the dynamic ocean replaced by an idealized slab ocean model (SOM; Bitz et al. 2012). The SOM includes a mixed layer ocean model, in which the mixed layer depth varies in space but not in time. The SOM lacks dynamic ocean processes present in the fully coupled model, and the ocean mixed layer is only thermodynamically coupled to the overlying atmosphere through air–sea heat fluxes (Bitz et al. 2012). Consequently, SOM experiments can simulate unrealistically high SST variability due to the lack of ocean damping processes (Murphy et al. 2021; Liu et al. 2023). By definition, the contribution from the anomalous wind stress (τ')–driven ocean circulation variability to HCS variability, which is critical to coupled modes like ENSO, Indian Ocean dipole (IOD), and Atlantic Niño, is excluded in SOM experiments. Therefore, in comparing fully coupled and SOM model results, it is difficult to determine whether the impact of the ocean circulation on HC variability is strictly due to the presence of these tropical coupled modes, enabled by τ'-driven ocean dynamics, or whether other ocean processes absent in the SOM (e.g., seasonally varying mixed layer depth and advection by mean ocean circulation) modulate SST variations that then feedback onto the atmospheric circulation.

In this study, we apply a rigorous experimental framework of the Community Earth System Model, version 2 (CESM2), to address the following questions: (i) How much variability of the HCS is internally coupled to the anomalous wind stress (τ')–driven ocean variability versus eddy-driven atmospheric variability? (ii) How much variability of the HCS is directly linked to ENSO variability? We also aim to determine if these potential drivers of HCS variability operate in one or both hemispheres.

The organization of the paper is as follows. Section 2 describes the datasets, model experiments, analysis methods, and definitions used in this study. Section 3 presents the research findings separately for the Northern and Southern Hemispheres, followed by presenting hypotheses regarding the asymmetric ENSO impact on the HCS variability. Section 4 provides the summary and discussion of this work.

2. Data and methods

a. Reanalysis datasets

In this study, we analyze both climate models and atmospheric reanalysis datasets. Three different atmospheric reanalysis datasets are used: (i) the fifth major global reanalysis produced by European Centre for Medium-Range Weather Forecast (ECMWF) (ERA5; Hersbach et al. 2020), (ii) the NCEP–NCAR reanalysis (Kalnay et al. 1996) from years 1950 to 2022, and (iii) the Japanese 55-yr Reanalysis (JRA-55; Kobayashi et al. 2015) from years 1958 to 2022. The NCEP–NCAR reanalysis dataset has a spatial resolution of 2.5° with 17 pressure levels. The JRA-55 dataset has a spatial resolution of 1.25° with 37 pressure levels, and the ERA5 dataset has a higher resolution with a 0.25° horizontal resolution and 37 pressure levels.

b. Model experiments

We consider preindustrial simulations of the CESM2 (Danabasoglu et al. 2020). The preindustrial simulation of the CESM2 model is forced with a constant radiative forcing from the year 1850 and thus exhibits no response to external forcing. To understand the effects of τ'-driven ocean circulation variability on the HCS variability, we use a hierarchy of coupled model experiments from the CESM2 base model. Each model version has a nominal 1° horizontal grid resolution. The model experiments employed in this study are described in order of decreasing complexity and are as follows.

1) FC CESM2

The fully coupled (FC) version of the CESM2 consists of dynamical atmosphere and ocean model components and land and sea ice components, coupled to each other. The coupling between the dynamic ocean and atmosphere occurs through (i) buoyancy fluxes, defined as the net air–sea heat fluxes and freshwater fluxes (Q_{buoy}), and (ii) momentum fluxes (Q_τ), which represent the momentum transfer from the atmosphere to the ocean through wind stress. Ocean variability is generated through the anomalous component of the buoyancy (Q'_{buoy}) and momentum fluxes (Q'_τ). Hence, tropical SST variability in the FC model is primarily governed by both anomalous thermodynamics and anomalous τ'-driven ocean dynamics.

2) MD CESM2

The mechanically decoupled (MD) model shares identical model components with the FC model where the anomalous momentum coupling is disengaged over the global ocean. In the MD model, the ocean is forced by climatological 6-hourly wind stress ($\bar{\tau}$) from the fully coupled model simulation; thus, MD lacks τ'-driven ocean circulation variability (Larson et al. 2024; McMonigal and Larson 2022). As a result, the atmosphere cannot strengthen the initial SST anomaly in the ocean through the τ'-driven ocean circulation (i.e., Bjerknes feedback) to support the development of τ'-driven dynamic ocean modes such as ENSO, IOD, and Atlantic Niño. The primary drivers for tropical SST variability in the MD model are, therefore, the advection of anomalous SST by the mean ocean circulation and anomalous thermodynamic forcing. The MD model differs from a climate model coupled to a SOM, in which SST variability is driven only by thermodynamic forcing. Further, the MD includes a seasonally varying mixed layer depth. For a comprehensive understanding of the MD model, readers should refer to Larson et al. (2024).

3) NoENSO CESM2

The NoENSO model is similar to the MD model except that the tropical Pacific Ocean only lacks the τ'-driven ocean circulation variability instead of the global ocean to suppress ENSO variability (Larson and Kirtman 2015; McMonigal and

Larson 2022). Figure S1 in the online supplemental material shows the tropical Pacific region (10°N–10°S, 120°E–60°W) over which the mechanical decoupling is applied in the NoENSO model. As a result, only ENSO variability is suppressed in this model because of disengaging the Bjerknes feedback facilitated through τ'-driven ocean circulation in the tropical Pacific. Outside the equatorial Pacific, the NoENSO model exhibits ocean–atmosphere coupling similar to that of the FC model.

To verify that mechanically decoupling the tropical Pacific indeed removes ENSO variability, we show the Niño-3.4 index for the above three CESM2 model experiments in Fig. S2. The FC clearly exhibits interannual ENSO variability, while the MD and NoENSO do not. Further diagnostics on the removal of ENSO using this approach can be found in McMonigal and Larson (2022) and Sutton et al. (2024) for a predecessor version of CESM2 and Larson et al. (2024) for CESM2. In summary, the difference in HCS variability between FC and MD models captures the overall contributions of τ'-driven ocean circulation variability, including ENSO, to HCS variability. The difference between FC and NoENSO indicates the contribution of only ENSO to HCS variability. The difference between NoENSO and MD indicates the role of τ'-driven ocean circulation variability outside the tropical Pacific. In this study, we mostly compare FC and MD models to determine the role of τ'-driven ocean circulation variability in HCS variability. We further compare FC and NoENSO models to determine the extent to which ENSO contributes to the τ'-driven ocean circulation variability.

c. Definitions and analysis methods

The variables used across the reanalysis and model datasets consist of monthly mean horizontal and vertical wind components, SST, air temperature, surface heat fluxes, sea level pressure (SLP), and net shortwave and longwave fluxes at the top of the atmosphere. We also use daily zonal and meridional velocity components to understand the atmospheric eddy dynamics. We utilize 600 model years for both daily and monthly mean variables for the FC model. For the MD, we have 600 years of monthly variables and 100 years of daily variables. For the NoENSO model, we use monthly variables across 500 available model years.

1) HC

We define the HC using the definition of the zonal-mean meridional streamfunction (ψ) by integrating the zonal-mean meridional wind based on the continuity equation (Peixoto and Oort 1992),

$$\psi = \int_{P_s}^{0} \frac{2\pi a \cos\phi}{g} v \partial p, \tag{3}$$

where v is the zonal-mean and annual-mean meridional wind, p is the pressure, ϕ is the latitude, a is Earth's radius, and g is the gravity. In Eq. (3), a positive ψ value indicates a clockwise meridional overturning circulation, and a negative value indicates a counterclockwise meridional overturning circulation.

2) HCS

HCS in each hemisphere is defined as the maximum absolute value of ψ between the Hadley cell edge and the location of the ITCZ across the vertical levels (Zhou et al. 2020). The location of the ITCZ is defined as latitude near the equator where ψ is zero at the 500-hPa level. The location of the HC edge is calculated using the PyTropD Python package (Adam et al. 2018), where the edge is defined in each hemisphere where ψ changes sign poleward of the tropical streamfunction maxima.

3) WINTER-VS-SUMMER–CENTERED ANNUAL MEAN

To analyze the year-to-year variability of the HCS, we compute annual means either centered on the boreal summer months (hereafter summer-centric) or the boreal winter months (hereafter winter-centric). Given that ENSO peaks during the boreal winter months of November through February, the summer-centric annual mean taken from January to December can include two different ENSO events and potentially average out their differing impacts on the HCS. To avoid this issue and given our interest in quantifying the ENSO influence on the interannual HCS variability, we employ the winter-centric annual mean by taking the annual mean from July of a given year to June of the next, centered on December and January. The key results obtained from the summer-centric annual mean are qualitatively similar and are provided in Fig. S3.

4) ANALYSIS METHODS

Monthly anomalies are calculated by subtracting the monthly climatology at every grid point. Eddy velocities are defined as the deviations from the daily climatological zonal-mean velocities. To identify patterns associated with the HCS variability (i.e., stronger or weaker HCS), we use composite analysis. The stronger HCS composite years are identified when the anomalous annual-mean HCS exceeds the 90th percentile of the annual-mean HCS anomaly distributions. Similarly, we identify the weaker HCS composite years when the anomalous annual-mean HCS is less than the 10th percentile of the annual-mean HCS anomaly distributions. We use Pearson's correlation coefficient to assess the correlation between variables. A significance level of 95% is employed for statistical tests unless explicitly stated otherwise. The annual-mean Niño-3.4 index is defined as the area-averaged SST anomalies over 5°S–5°N, 170°–120°W.

3. Results

a. Mean HC

We first compare the climatological mean HC between the FC and MD models and ERA5 using the zonal-mean streamfunction (ψ), as shown in Figs. 1a–c. The annual-mean HCs computed from the NCEP–NCAR and JRA-55 reanalysis datasets are consistent with the ERA5 reanalysis (see Fig. S4). The models and ERA5 show similar features, including a stronger and meridionally wider SH circulation compared to the NH circulation. Overall, CESM2 models exhibit a slightly stronger mean circulation intensity compared to the ERA5

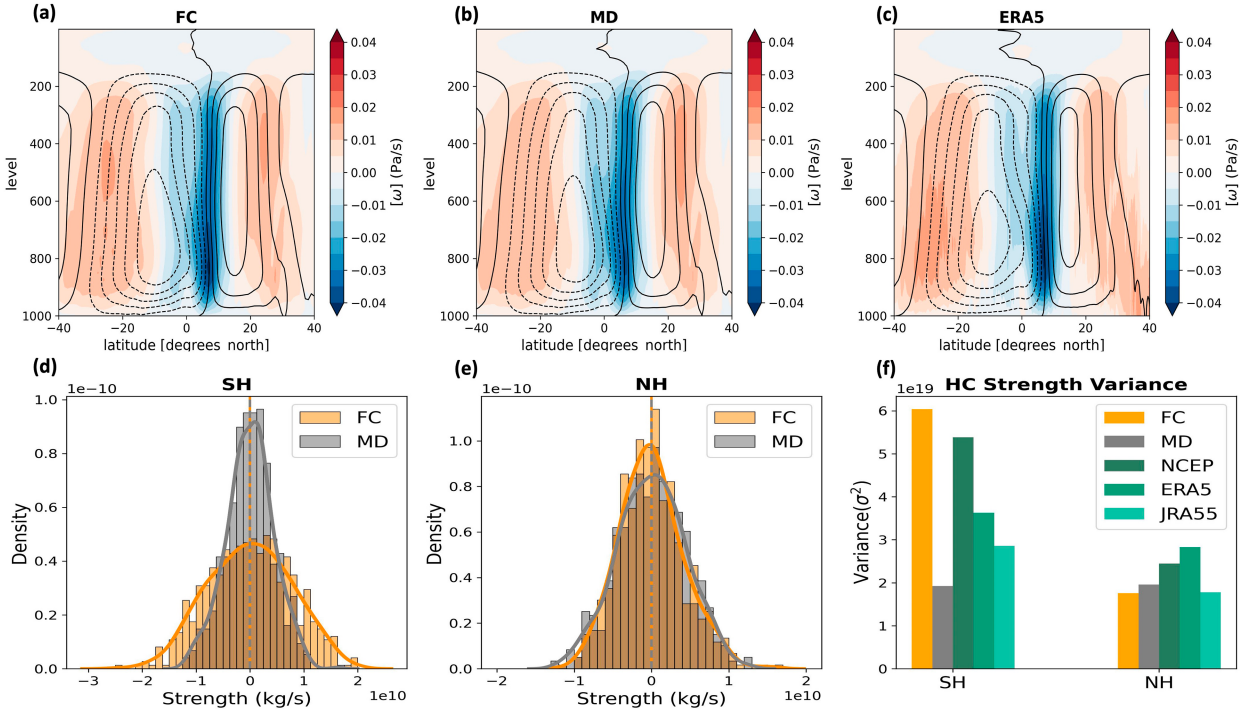

FIG. 1. Annual-mean HC in (a) FC model, (b) MD model, and (c) ERA5 reanalysis. Shadings represent vertical velocity in pressure coordinates (ω; Pa s^{-1}), and the contour lines indicate streamfunction (Ψ; kg s^{-1}). Blue and red shadings indicate upward and downward motions. Solid and dashed contours represent clockwise and counterclockwise circulations. (d),(e) Distribution of the annual-mean HCS anomaly in the Southern and Northern Hemispheres, respectively, for the FC (orange) and MD (orange). (f) HCS variance in each hemisphere for both models and reanalyses (kg^2 s^{-2}).

(see Figs. S4c,d) although the boundary of the HC aligns between the models and reanalysis. The similarity of the magnitude and spatial pattern of the HC between reanalyses and model results suggests that the CESM2 reasonably represents the zonal-mean HC in both hemispheres. The mean HCS in the MD is slightly weaker in the SH and stronger in the NH compared to the FC, as shown in Figs. S4c and S4d. This means that the absence of the τ'-driven ocean circulation variability in the MD reduces the mean circulation strength in the SH and increases the strength in the NH. We briefly investigate what causes the difference in the mean HCS in the CESM2 models.

To illustrate the differences in mean HCS between FC and MD models, Figs. 2a and 2b depict the mean differences in SST and air temperature between MD and FC models (e.g., MD − FC). Both SST and air temperature are relatively warmer in the SH than the NH in the MD although both hemispheres are generally warmer in the MD compared to the FC (McMonigal et al. 2023). The warmer SST in the MD than that in the FC is consistent with the shoaling of the ocean mixed layer in the MD and the resulting warming of the mixed layer temperature due to the lack of τ'-driven mixing and entrainment of cold water from below (Luongo et al. 2024; Larson et al. 2024). The warmer SST then induces upper-tropospheric warming (Fig. 2b) through upward heat transport by the atmospheric circulation. As a result, there is a hemispheric imbalance of the heat within the atmosphere, which requires a cross-equatorial energy transfer to balance the energy in the MD (Fig. 2c). This energy transport occurs through the tropical meridional atmospheric circulation, i.e., HC, following the energetic framework (Kang et al. 2008; Frierson et al. 2013; Schneider et al. 2014; Kang et al. 2014; Kang 2020). Figure 2d shows the differences in HC (black contours) and vertical velocity (shading) between the models. The hemispherical asymmetric warming pattern in the MD induces a southward shift of the ITCZ, which corresponds to the areas of low-level convergence and rising motion. This excess energy from the SH is then transported to the NH through a positive (clockwise) HC, as shown by the positive streamfunction in Fig. 2d.

b. *Interannual HCS variability*

To confirm that the CESM2 reproduces the observed HCS variability, we compare the interannual HCS variability between the CESM2 FC model and the reanalyses for each hemisphere in Fig. 1f. The HCS variability in the SH is clearly larger than that in the NH in both the CESM2 FC model and reanalysis datasets, consistent with Tanaka et al. (2004) and Chemke (2022). The hemispheric asymmetry in the HCS variability is also observed in the CESM2 historical ensembles as shown in Fig. S5. Further, the CESM2 model's ability to reproduce the interhemispheric asymmetry in HCS variability validates its use in the present study. Note that the magnitude

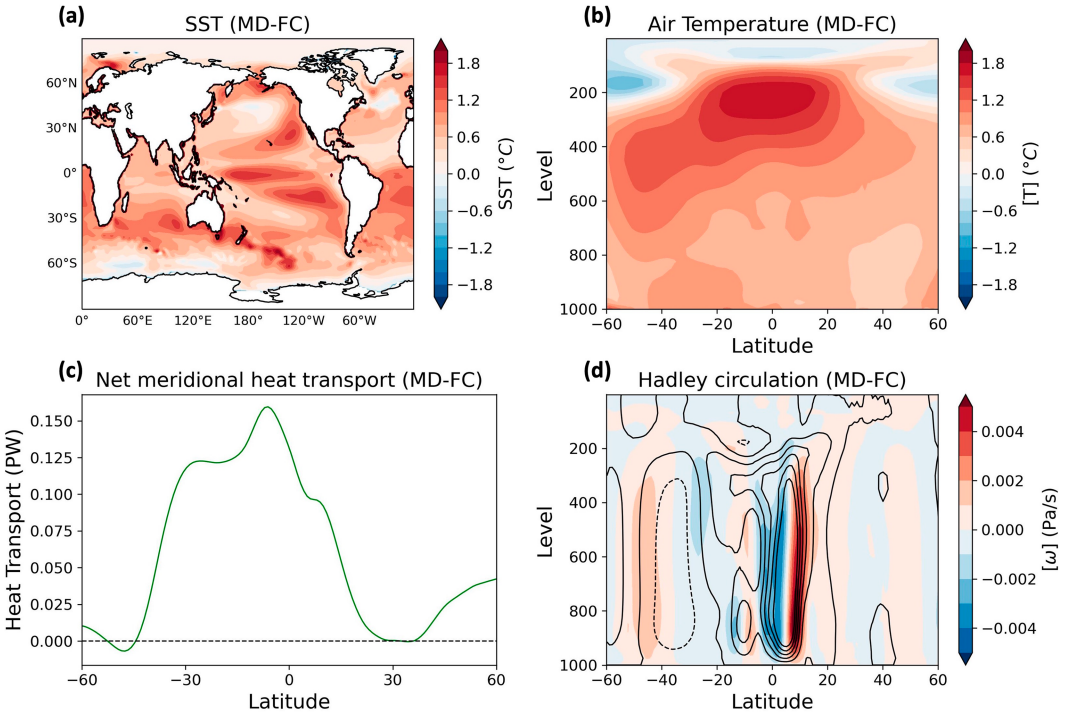

FIG. 2. Annual-mean difference between CESM2 FC and MD models: (a) SST (°C), (b) zonally averaged air temperature (°C), (c) net meridional heat transport by the atmosphere (PW), and (d) HC with the shading indicating velocity in pressure coordinates ω (Pa s^{-1}) and contour lines representing meridional streamfunction ψ (kg s^{-1}).

of the HCS variability can differ among the reanalysis datasets, as shown in Chemke (2022).

Comparing the HCS variability between the FC and MD models indicates that the τ'-driven ocean circulation variability significantly increases the HCS variability in the SH but not in the NH (Figs. 1d–f). Given that the mechanism by which the ocean modulates HC variability begins through interactions with the SST (Clement 2006; Chemke and Polvani 2018; Zhou et al. 2020; Chemke 2022), this result implies an interhemispheric asymmetry in the impact of τ'-driven SST variability on the HCS variability. To understand the mechanism of the HCS variability and the potential role of the τ'-driven ocean circulation variability, we further investigate the interannual variability of the HCS in each hemisphere separately.

1) NH VARIABILITY

The NH exhibits a similar amount of HCS variability between the FC and MD (Figs. 1e,f), indicating that τ'-driven ocean circulation variability does not substantially modulate the NH HCS variability. Therefore, internal atmospheric variability is likely the primary driver of the NH HCS variability. We know that tropospheric eddies can influence atmospheric circulation through meridional exchange of energy and momentum (Vallis 2017). According to Eq. (1), the divergence of the eddy momentum flux can influence the HC mass flux through the meridional advection of absolute angular momentum in the upper troposphere. Hence, to identify the potential eddy influence on the HCS variability, we calculate the eddy momentum flux divergence at the 200-hPa level in both models to compare and correlate with the interannual HCS anomaly.

Figures 3a and 3b present the mean upper-level eddy momentum flux divergence anomaly for strong and weak NH HCS composites. As we have 100 years of daily data available from the MD model, we have subdivided the 600 years of FC datasets into six nonoverlapping segments, each consisting of 100 years. We then compute composite mean eddy momentum flux divergence anomalies for the six different segments. The shadings in Figs. 3a and 3b represent one standard deviation (std) spread of the segmented datasets from the FC mean. For a strong NH HC (Fig. 3a), the eddy momentum flux anomaly in both models diverges in the NH subtropics and converges in the midlatitudes, and for a weak NH HC (Fig. 3b), the eddy momentum flux anomaly converges in the subtropics and diverges in the midlatitudes. The correlation between the NH HCS and the divergence of subtropical (averaged over 10°–25°N) eddy momentum flux anomaly is illustrated in Fig. 3d. FC (orange open circles) and MD (black open circles) both show a statistically significant correlation between the HCS anomaly and the divergence of subtropical eddy momentum flux anomaly with a correlation coefficient value of 0.70 and 0.78, respectively. This result suggests that upper-tropospheric eddies strongly modulate the interannual NH HCS variability, consistent with Caballero (2007).

Given that the relationship between atmospheric eddies and NH HCS is similar between the FC and MD, as is the

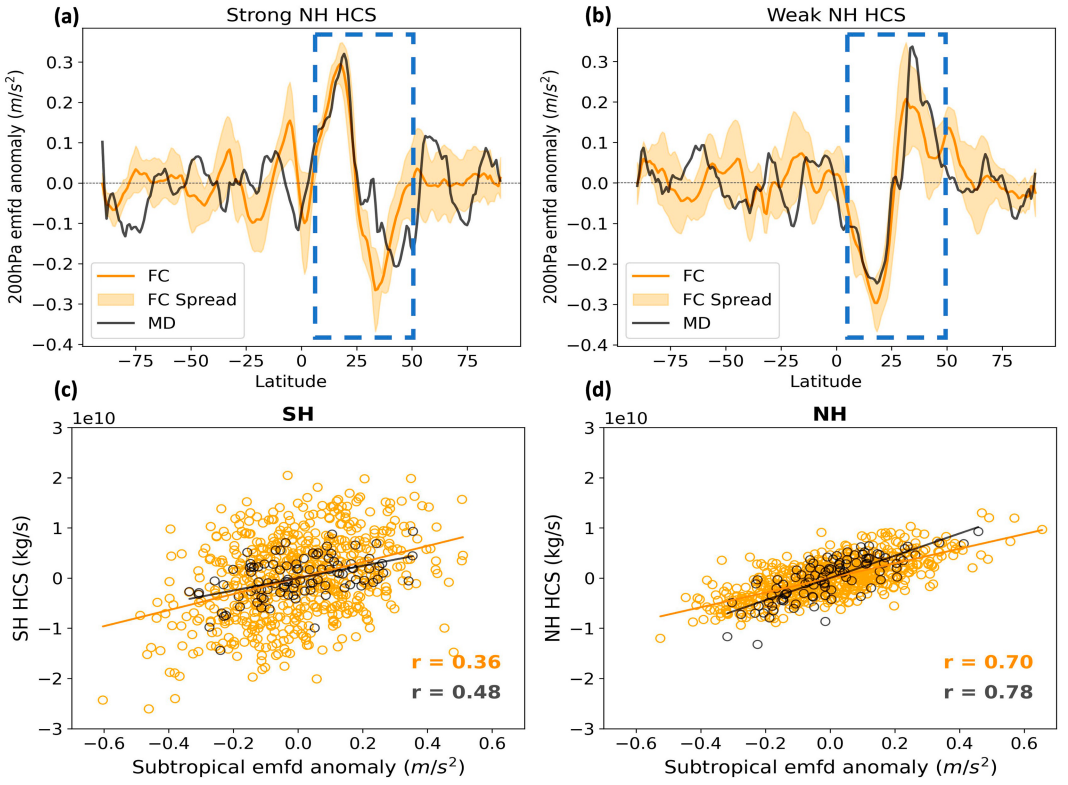

FIG. 3. Composite mean of 200-hPa EMFD anomalies (m s^{-2}) for (a) strong and (b) weak NH HCS years. The FC data are subdivided into six 100-yr nonoverlapping segments to match the length of the available MD dataset of daily data. The shading represents a 1 std spread from the mean FC result (dark orange line), as computed from the six segments of the FC model output. The blue dashed rectangle highlights the subtropics and midlatitudes in the NH. The scatterplot between HCS and subtropical (averaged over 10°–25° latitudes) EMF divergence anomalies and the corresponding least squares linear fit lines are shown for both the (c) SH and (d) NH, and the corresponding correlation coefficient (r) values are shown in the bottom-right corner. Orange and gray colors represent the results from the FC and MD models, respectively.

overall magnitude of HCS variability (as seen in Figs. 1e,f), we expect similar tropospheric circulation patterns associated with strong and weak NH HCs in both the FC and MD. Figure 4 illustrates the composite mean difference between strong and weak NH HC [(strong − weak)/2] for both FC and MD models, highlighting the anomalous zonal-mean streamfunction, zonal wind, and SST. The sign of the anomalies in each panel reflects the climate anomalies associated with an anomalously strong NH HC. By definition, the patterns show the linear component of the composite differences; therefore, a weaker-than-usual HC would be associated with climate anomalies of the opposite sign to Fig. 4. The nonlinear component is generally an order of magnitude smaller than the linear component (not shown). In the FC, a positive circulation (clockwise) anomaly reinforces the climatological circulation to result in a stronger HC in the NH (Fig. 4a). The zonal-mean zonal wind anomaly pattern (Fig. 4c) also generally enhances the climatological pattern when the NH HC is anomalously strong. In the MD (right panel), a stronger NH HC is linked to similar composite anomaly patterns as the FC model (Figs. 4b,d,f) although the HC anomaly pattern in the MD (Fig. 4b) exhibits a meridionally broader spatial pattern than in the FC. The zonal-mean zonal wind anomaly in Fig. 4d resembles the pattern from the FC, particularly in the NH tropics, with a reinforcement of the subtropical westerly jet and lower-tropospheric easterlies.

In both the FC and the MD, a stronger NH HC is accompanied by cool subtropical SST anomalies (Figs. 4e,f) that resemble the negative phase of the thermodynamically driven North Pacific meridional mode (NPMM; Chiang and Vimont 2004), which is typically forced by internal atmospheric variability originating in the extratropics (Vimont et al. 2003). The strong upper-level subtropical eddy divergence induces a stronger NH HC (Figs. 4a,b), intensifying surface prevailing winds stemming from the lower branch of the HC (Figs. 4c,d). This intensification of the surface wind then leads to increased latent and sensible heat fluxes from the ocean (not shown) and subsequent cooling of the SST (Figs. 4e,f). This cooling is more effective in the MD because τ'-driven ocean advection, which is active in the FC, has been shown to damp the thermodynamically driven SST associated with the NPMM (Shu et al. 2023). Conversely, for a weak NH HC, a weakening of the easterly wind would lead to a decrease in the air–sea heat exchange and warm subtropical SST anomaly.

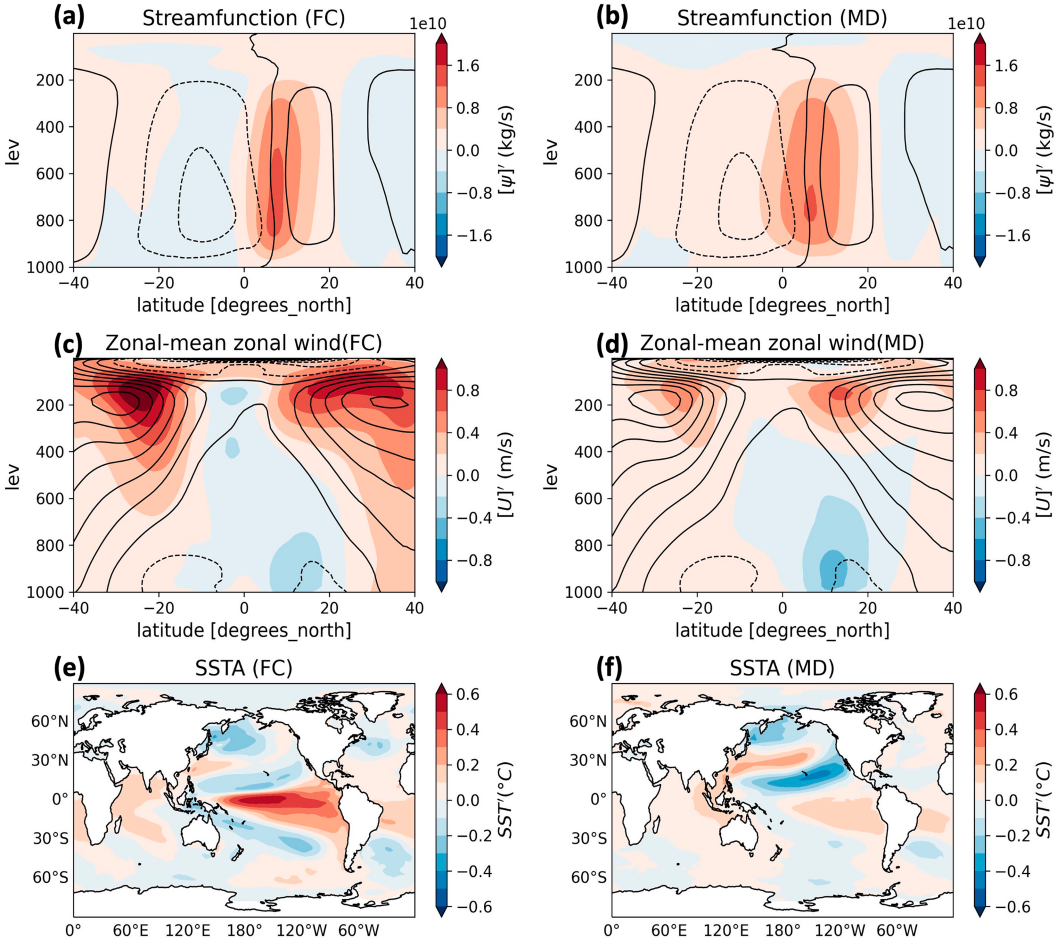

FIG. 4. Linear component of the strong NH HCS composite anomalies, computed by taking the difference between strong and weak NH HC (strong − weak/2) composite means. Composite mean from the (left) FC and (right) MD models, illustrating the (a),(b) meridional streamfunction; (c),(d) zonal wind; and (e),(f) SST anomalies associated with a stronger NH HC. Shading in each panel represents the anomalous term, and the contours shown in (a)–(d) show the climatological mean from the respective models. The contour intervals of the climatological meridional streamfunction and zonal wind are 5×10^{10} kg s^{-1} and 5 m s^{-1}, respectively.

In the tropics, the FC SST anomaly pattern resembles a central Pacific El Niño, whereas the relatively weaker tropical warming signal in the MD compared to the FC is consistent with a lack of warming via the zonal advective feedback, which is critical to the generation of central Pacific El Niño events (Capotondi et al. 2015). Both the NPMM and central Pacific El Niño events have a strong connection to internal extratropical atmospheric circulation variability (Pegion et al. 2020); therefore, we expect that the SST anomaly pattern and NH HCS in the FC are both driven by a common atmospheric forcing, rather than the tropical SST anomaly contributing to the HCS.

2) SH VARIABILITY

Unlike the NH HCS variability, the SH HCS exhibits noticeably higher variability in the FC compared to the MD, indicating that τ'-driven ocean circulation variability modulates the HCS in the SH (Figs. 1d,f). This is further supported by Fig. 3c, which indicates only a modest correlation between eddies and the SH HCS, thus suggesting processes other than eddies are important contributors to HCS in the SH. To better understand the τ'-driven climate patterns associated with stronger and weaker SH HCS, Fig. 5 illustrates the linear composite anomaly of the strong SH HCS for both models, similar to Fig. 4. A stronger SH HC in the FC, as illustrated by the anomalously negative meridional streamfunction (shading in Fig. 5a), reinforces the climatological counterclockwise circulation (dashed contour lines) in the SH. The anomalous circulation pattern is symmetrical about the equator, characterized by an ascending branch near the equator and descending branches on the poleward flanks in both hemispheres. When the SH HC is anomalously strong, the anomalous zonal wind in the FC model (Fig. 5c) also reinforces the climatological mean easterly winds in the tropics and westerlies in the midlatitudes. A strengthening of the zonal-mean

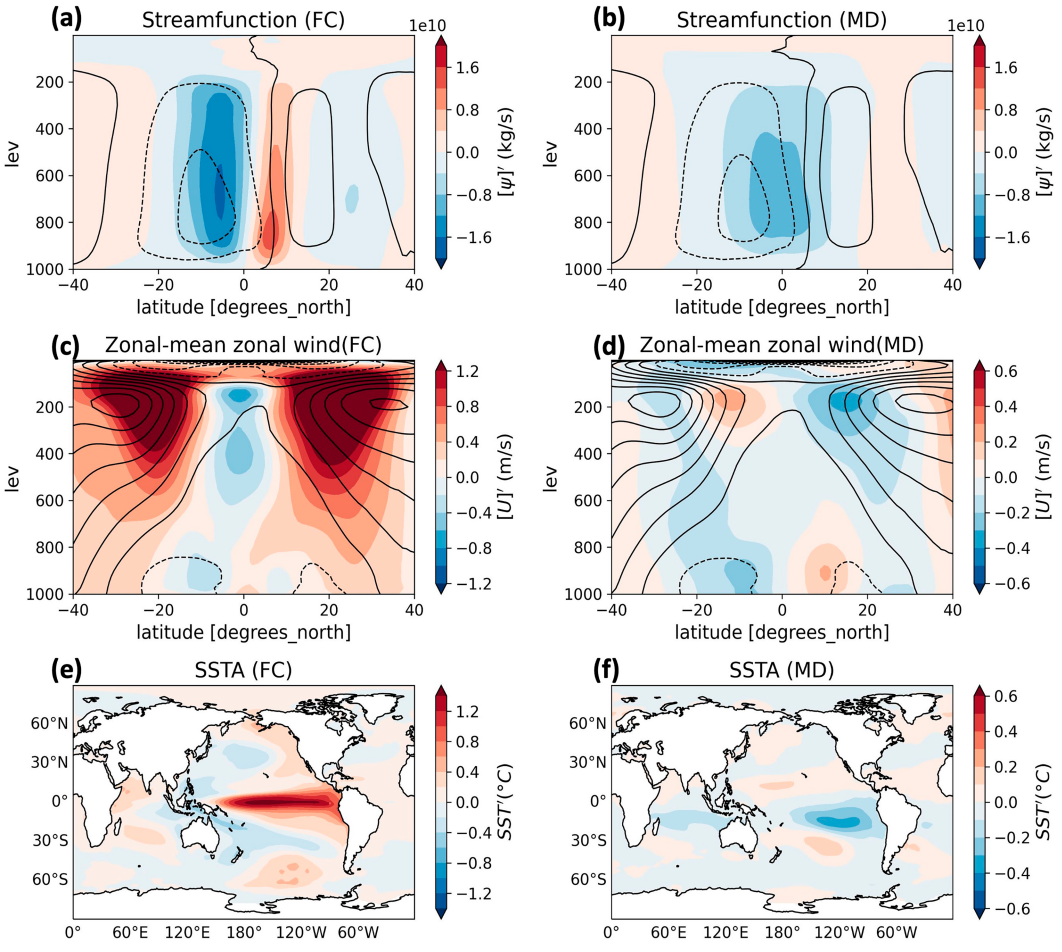

FIG. 5. Linear component of the strong SH HCS composite anomalies, computed by taking the difference between strong and weak NH HC (strong − weak/2) composite means. Composite mean from the (left) FC and (right) MD models, illustrating the (a),(b) meridional streamfunction; (c),(d) zonal wind; and (e),(f) SST anomalies associated with a stronger NH HC. Shading in each panel represents the anomalous term, and the contours shown in (a)–(d) show the climatological mean from the respective models. The contour intervals of the climatological meridional streamfunction and zonal wind are 5×10^{10} kg s^{-1} and 5 m s^{-1}, respectively.

zonal wind is consistent with so-called El Niño–like symmetric climate variability (Seager et al. 2003; Robinson 2006). Similarly, a symmetric HC pattern is associated with the ENSO phases (Schneider and Bordoni 2008; Dima and Wallace 2003; Feng et al. 2016). The SST anomaly associated with a stronger SH HC, as illustrated in Fig. 5e, shows a canonical El Niño pattern in the equatorial Pacific. The sea level pressure anomaly (SLPA) shown in Fig. S6 depicts the dipole pattern in the tropical Pacific typically associated with canonical El Niño. We further investigate the relationship between ENSO and the SH HCS by computing the correlation between the Niño-3.4 index and the SH HCS, as shown in Fig. 6a. A statistically significant correlation between Niño-3.4 and the SH HCS in the FC is observed with a correlation coefficient of 0.74 (orange open circles). A similar but opposite argument exists for the La Niña events and associated weak HCS in the SH.

Alternatively, a strong SH HCS in the MD (Figs. 5b,d,f) shows a distinctly different climate pattern than the FC. The anomalously strong HC in the MD illustrated by the negative streamfunction (shading in Fig. 5b) is asymmetrical about the equator, featuring an ascending branch in the NH and a descending branch in the SH. The zonal-mean zonal wind anomaly also shows a distinct hemispherical pattern with an enhanced subtropical jet in the SH and a weakened one in the NH. The SST anomaly pattern associated with a strong SH HC in the MD model (Fig. 5f) also differs from that in the FC and shows broad cooling restricted to the eastern Pacific. Since the HCS variability in the MD lacks the influence of the τ'-driven ocean, the SST anomaly is primarily associated with the thermodynamic forcing. In fact, the cool SST anomaly pattern shown in Fig. 5f resembles the negative phase of the South Pacific meridional mode (SPMM), a thermodynamically driven coupled mode that originates in the southeast Pacific and is similar to the NPMM (Zhang et al. 2014; Larson et al. 2018; Amaya 2019). As the MD lacks ENSO variability, the correlation between the Niño-3.4 index and the SH HCS can result from the weak

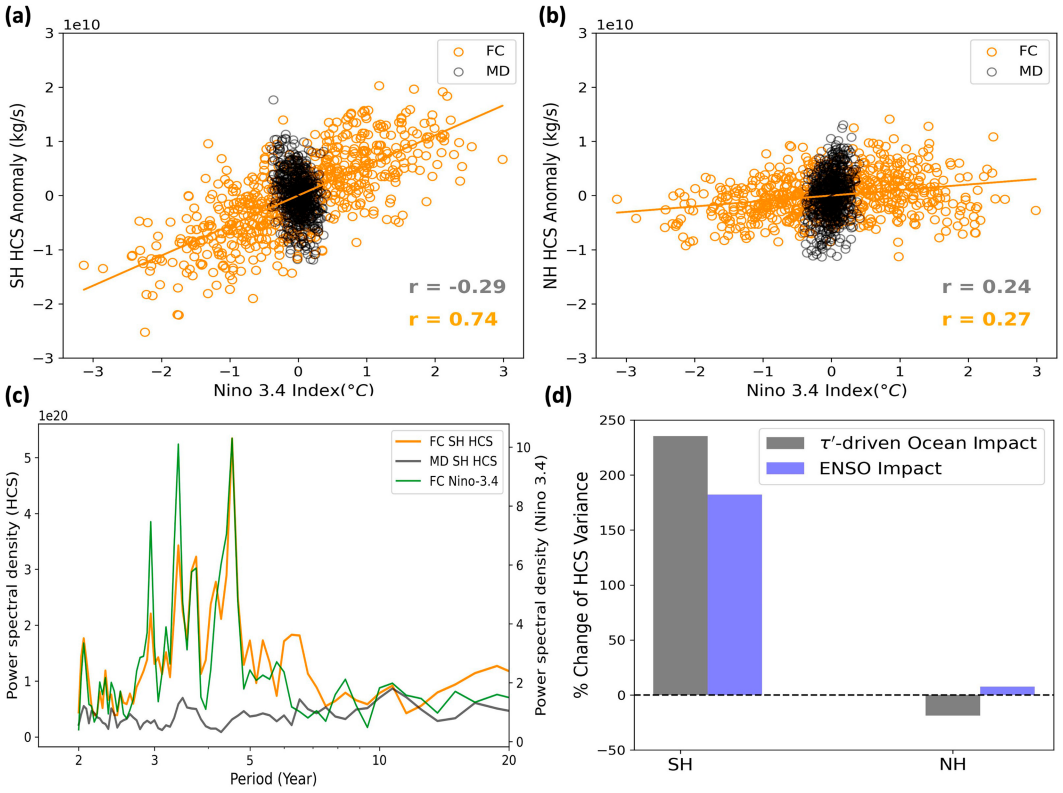

FIG. 6. Scatterplot between the anomalous annual-mean HCS (kg s^{-1}) and the Niño-3.4 SST anomalies in (a) NH and (b) SH for the MD and FC. The solid lines show corresponding linear fit lines, whereas the correlation coefficient (r) values between HCS and the Niño-3.4 SST anomalies are shown in the bottom-right corner. (c) Power spectral density of the SH HCS from the FC and MD models and Niño-3.4 index from the FC model (green color). (d) Percentage change in variance of the HCS between the models for each hemisphere. The percentage difference between FC and MD variance (normalized by the MD variance) shown by the gray bar denotes the impact of overall τ'-driven ocean circulation. The percentage difference between FC and NoENSO variance (normalized by the NoENSO variance) shown by the blue bar denotes the impact of ENSO.

influence of the negative SPMM extending into the Niño-3.4 region. Figure 6a (black open circles) shows a statistically insignificant yet negative correlation ($r = -0.29$) between the SH HCS and the Niño-3.4 index for the MD model. This is consistent with the negative SST anomalies associated with the negative phase of SPMM that appear in the strong SH HCS composite. Additionally, a statistically significant correlation ($r = 0.48$) between SH HCS and subtropical eddies shown in Fig. 3c suggests that similar to the NH, an enhanced upper-atmospheric eddy activity induces a strong SH HC (Fig. 5b) and strong surface easterlies (Fig. 5d) to cool the SST in the tropics. Hence, internal atmospheric variability could act as a common driver for both SPMM and SH HCS as such; the SST anomaly in Fig. 5f shows a pattern similar to the SPMM.

It is evident that the τ'-driven ocean circulation variability, primarily associated with ENSO, substantially enhances the HCS variability in the SH but not in the NH. In Fig. 6c, the power spectra of Niño-3.4 and the SH HCS time series from the FC model show the highest variability on interannual time scales consistent with ENSO, whereas the MD shows no peak on interannual time scales. However, the extent to which ENSO solely contributes to the enhanced SH HCS variability in the FC model is still unknown because the MD model lacks not only ENSO but also the IOD and Atlantic Niño, as well as τ'-driven ocean circulation variability in the extratropics.

To identify the sole contribution from ENSO to HCS variability, we repeat the analysis using the CESM2 NoENSO model (see section 2 for details). Recall that the NoENSO experiment is similar to the FC but lacks ENSO variability. Figure 6d shows the overall contribution of the τ'-driven ocean circulation (i.e., FC − MD) and ENSO (i.e., FC − NoENSO) to the SH HCS variance. The τ'-driven ocean circulation increases the SH HCS variability by approximately 2.4 times, while ENSO alone contributes to the majority (roughly 80%) of that enhancement. Hence, it is clear that the difference in the SH HCS variance between FC and MD, as illustrated in Fig. 1f, mostly originates from ENSO. The remaining SH HCS variability, which is not related to ENSO (roughly 20%), may arise from a combination of factors, including the IOD, Atlantic Niño, and wind-driven ocean variability from the extratropics. Conversely, the ENSO impact on the NH HCS variability is limited and accounts for less than 10% of the

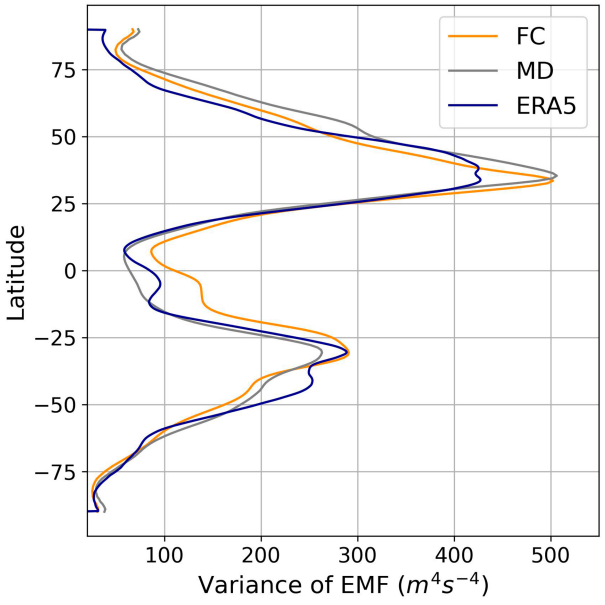

FIG. 7. Zonal-mean variance of the EMF (m^4 s^{-4}). The orange, gray, and blue colors represent the CESM2 FC, CESM2 MD, and ERA5, respectively.

variability. Figure 6b further confirms the inconsequential relationship between ENSO and the NH HCS in both FC (r = 0.27) and MD (r = 0.24). Instead, eddy-driven internal atmospheric variability primarily modulates the HCS variability in the NH.

It is important to highlight that the SH HCS also shows a relatively weak correlation with the upper-level eddies compared to the NH in both models, as seen in Fig. 3c. In the SH, eddies and HCS are more highly correlated in the MD that lacks ENSO (r = 0.48) than in the FC (r = 0.36), suggesting that in the absence of ENSO, eddy variability is a stronger predictor of the SH HCS compared to when ENSO is active (as in the FC). Hence, we hypothesize that the upper-level eddies still play an important role in the SH HCS variability but that the additional impact from ENSO in the FC may obscure the impact of eddies in the SH compared to the NH. This is further evidenced by the smaller spread about the least squares linear fit line in the MD compared to the FC for the SH HCS (Fig. 3c). Similarly, the spread about the linear fit line for the NH in both models (Fig. 3d) is smaller than that in the FC for the SH, further suggesting that ENSO plays a uniquely important role in modulating the SH HCS variability.

3) HEMISPHERE-DEPENDENT ENSO IMPACT

We find a hemisphere-dependent ENSO impact on the interannual HCS variability with a strong influence in the SH and little-to-no influence in the NH. We hypothesize this result is twofold: (i) the NH exhibits more eddy variability than the SH and (ii) ENSO-related heating primarily originates in the SST underlying the SH HC rather than the NH HC. Figure 7 shows the variance of the zonal-mean eddy momentum fluxes at 200-hPa level in models and ERA5 reanalysis. Both models and reanalysis show a relatively higher eddy momentum flux variance in the NH compared to the SH, consistent with the relatively more variable NH storm tracks (Wettstein and Wallace 2010).

The atmospheric response to the ENSO heating anomalies is symmetric about the equator (Seager et al. 2003, 2005; Robinson 2006). However, the annual-mean ITCZ position, which is concomitant with the ascending branch of the HC, lies north of the equator around 7°, as shown by the thick black line in Fig. 8. We hypothesize that the annual-mean ITCZ location can explain why ENSO more strongly impacts the SH, rather than NH, HCS variability. Figure 8 illustrates the SST and precipitation anomaly patterns (Fig. 8a) and the zonal-mean streamfunction anomaly (Fig. 8c) pattern associated with ENSO, calculated by regressing the corresponding variables onto the Niño-3.4 index. The patterns are consistent with those in Figs. 5a and 5e for the strong SH HCS composites in the FC model. Due to the collocation of the mean HC's ascending branch with the ITCZ (as depicted in Fig. 8c), ENSO heating anomalies (Fig. 8a) in the equatorial Pacific are predominantly collocated with the SH HC. Consequently, the ENSO-related precipitation anomalies (blue contours in Fig. 8a) shown as a proxy to ENSO-related column-integrated latent heating are also located in the SH. Hence, during El Niño, the ENSO-related thermally driven anomalous circulation (shadings in Fig. 8c) reinforces the climatological streamfunction (contours in Fig. 8c) maxima only in the SH but not in the NH. The opposite is true for La Niña. Note that in Fig. 8c, both positive and negative streamfunction anomalies impact the NH cell, leading to a muted ENSO impact.

4. Summary and discussion

While both ENSO and atmospheric eddies are known to modulate interannual variability in HCS, the relative contributions of these oceanic and atmospheric forcings to the HCS variability remains an open question. Moreover, the extent to which the τ'-driven ocean circulation variability, including ENSO, impacts the interannual HCS variability is unknown. To understand better the relative contributions of atmospheric and oceanic forcings and to quantify the role of τ'-driven ocean circulation variability in driving HCS variability, we investigate the drivers of the interannual HCS variability using the CESM2 model experiments that vary in the degree of air–sea processes included.

We find that the interannual HCS variability is driven by both oceanic and atmospheric forcings, and their relative contribution differs between the NH and SH. In particular, τ'-driven ocean circulation variability significantly increases the SH HCS variability by approximately 2.4 times in the CESM2 FC model when compared to the model version that lacks τ'-driven ocean circulation variability (i.e., CESM2 MD). ENSO is the leading modulator of the SH HCS variability, contributing roughly 80% impact of the overall τ'-driven ocean circulation variability. ENSO-induced thermal forcing in the tropics creates a strong meridional SST gradient to drive the HC in the SH. A greater response of the SH HCS to ENSO (or tropical Pacific SST) is consistent with Oort and Yienger (1996),

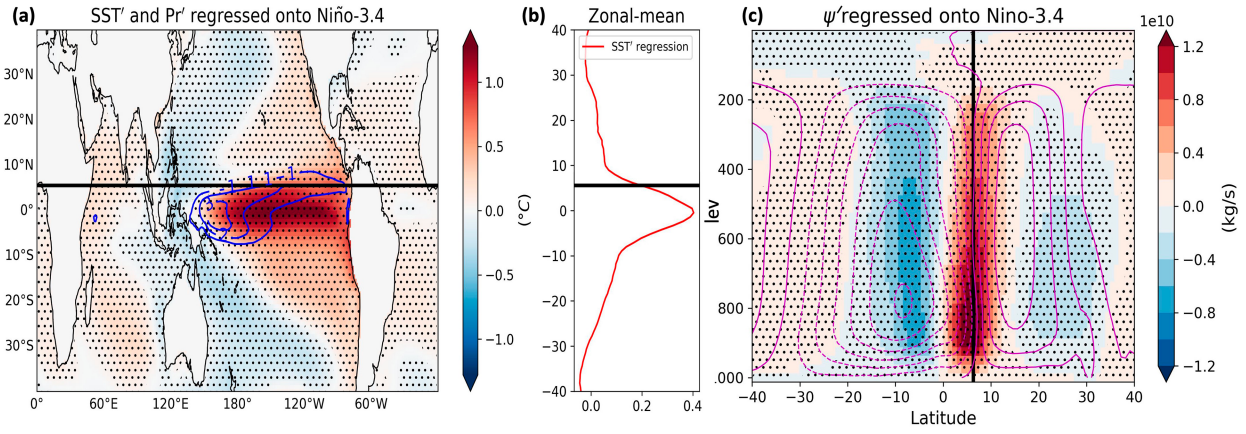

FIG. 8. (a) Anomalous SST (°C) and precipitation rate (mm day^{-1}) regressed onto the standardized Niño-3.4 index in the FC model, where shadings represent SST and blue contours represent precipitation (statistically significant at 95% confidence level) with a contour interval of 1 mm day^{-1}. (b) Zonal mean of the SST from (a). (c) Zonal-mean streamfunction anomalies (kg s^{-1}) regressed onto the standardized Niño-3.4 index (shadings). Magenta contours show the climatological mean HC with a contour interval of 2×10^{10} kg s^{-1}. Black dots in (a) and (c) indicate statistically significant regression coefficients at the 95% confidence level. The black solid line in each panel indicates the annual-mean ITCZ location.

Quan et al. (2004), and Zhou et al. (2020). Since ENSO variability is stronger in CESM2 than in observations (Capotondi et al. 2020), we expect a higher SH HCS variability in CESM2 than in observational reanalysis products as seen in Fig. 1f. Additionally, the limited length of the observational record may also potentially contribute to the discrepancy. On the other hand, the NH HCS variability is predominantly influenced by the eddy-driven internal atmospheric variability, with little role for τ'-driven ocean circulation variability. A strong eddy momentum flux divergence in the upper atmosphere drives a strong NH HC and vice versa. Subtropical surface wind stemming out of the lower branch of the HC consequently impacts surface variables including SST. We find that atmospheric eddies are also important in the SH, but the ENSO-induced thermal forcing dominates over the eddy forcing in the SH. Hence, the HCS variability is larger in the SH than in the NH, a result that is consistent with prior studies (Tanaka et al. 2004; Chemke 2022). We suggest two reasons why ENSO minimally impacts the NH HCS variability: (i) the NH exhibits more upper-atmospheric eddy variability compared to the SH (Fig. 7) and (ii) ENSO-associated heating and precipitation primarily originates in the SST underlying the SH HC rather than the NH HC (Fig. 8). Our results thus imply that the interannual variability of the HCS can be independent of each other, which is further supported by a significantly low correlation value ($r = 0.14$) between SH and NH HCS. Because of the uncertainty associated with the HCS definitions (Zurita-Gotor and Álvarez-Zapatero 2018; Pikovnik et al. 2022), we additionally test the sensitivity to the HCS definition by using HCS definition from Chemke and Polvani (2019). While the large hemispheric asymmetry in the HCS variability is insensitive to the HCS definition (shown in Fig. S7), it is possible that the combination of differences in the HCS definition and its annual mean, differences data sources, and differences in the time period analyzed might explain why some studies found an insignificant relationship between ENSO and HCS, especially in the SH.

These results also help elucidate how biases in models may contribute to their differences from historical HCS trends. For instance, the low-frequency coupled ocean variability associated with ENSO and Pacific decadal oscillation (PDO) can contribute significantly to the uncertainty in the historical HCS trend, particularly in the SH. Importantly, models that poorly simulate ENSO variability may underestimate or overestimate this uncertainty. Conversely, internal atmospheric variability may be the primary contributor to the uncertainty in the NH HCS trend associated with internal variability. In a future warmer climate, a projected increase in ENSO variability (Yun et al. 2021; Cai et al. 2022) may lead to increased SH HCS variability and to improved predictability in HC-related hydrology. ENSO response to future warming is, however, uncertain as Peng et al. (2024) found that the ENSO variance will decrease. Alternatively, the atmospheric static stability and meridional temperature gradients, both essential factors in generating midlatitude eddies (Held and Hoskins 1985; O'Gorman 2011; Holton and Hakim 2013), are also expected to change in a warming climate (Lu et al. 2008; Yuval and Kaspi 2020). Using models with projected warming scenarios, Yuval and Kaspi (2020) found that an increase in the static stability and a decrease in the meridional temperature gradient potentially weaken the upper-atmospheric eddy activities in the future climate. The projected changes in extratropical eddy activity are, however, sensitive to model resolution, and caution is required when interpreting climate change responses from low-resolution climate models (Willison et al. 2015). Since the interannual HCS variability is tied to both wind-driven ocean circulation and upper-level atmospheric eddy variability, future research should endeavor to quantify the change in the relative role of these ocean and atmospheric forcings to the hemispheric HCS variability in a warming climate. Furthermore, the interannual variability itself could change in a future climate.

The zonal-mean HC is a simplified portrayal of the real three-dimensional HC that neglects longitudinal variations. As

a result, to what extent ENSO and atmospheric eddies impact regional HCs is still unclear and necessitates future investigation. For instance, an important aspect of ENSO's regulation of SH HCS variability on interannual time scale is the potential for enhancing the predictability of related hydrological consequences. Hence, additional investigations are warranted to assess whether extreme HC intensity changes related to ENSO translate to more predictable low-latitude precipitation anomalies on a regional scale. Furthermore, we anticipate differences in the seasonal mean HCS variability compared to the annual mean. During El Niño, the zonal-mean ITCZ becomes narrower and shifts equatorward (Adam et al. 2016). This equatorward shift of ITCZ consequently moves the jet toward the equator, shrinks the HC (Lu et al. 2008), and allows midlatitude eddies to propagate further equatorward (Watt-Meyer and Frierson 2019). Hence, we might expect more symmetric ENSO influence on the HCS variability during boreal winter. While we focus our attention on the HCS variability, the variability of the HC edge is also important for the subtropical climate variability, with a potential influence on the SST variability (Hasan et al. 2022). Since the interannual variability of the HC edge is also influenced by both oceanic and atmospheric forcings (Frierson et al. 2007; Lu et al. 2008; Kang and Polvani 2011; Ceppi et al. 2013; Sun et al. 2019; Chemke and Polvani 2018; Li et al. 2023; Seo et al. 2023), our future research aims to examine and attribute the variability of the HC edge to both oceanic and atmospheric forcing using observations and model experiments.

Acknowledgments. We thank Dr. Spencer Hill and two anonymous reviewers for their thoughtful comments on this work. The research is supported by the NSF Grant AGS-1951713 (MH, SML, and KM). WAR is supported by NSF Grant AGS-2203515. We acknowledge Henry Goff for running the "CESM2 NoENSO" model experiment and sharing the related data and Fig. S1. We acknowledge NCSU high-performance computing support and high-performance computing support from Cheyenne (https://doi.org/10.5065/D6RX99HX) provided by NCAR's Computational and Information Systems Laboratory, sponsored by NSF.

Data availability statement. The ERA5 dataset is obtained from the Copernicus Climate Data Store (https://doi.org/10.24381/cds.6860a573), the JRA-55 dataset is obtained from the NCAR Climate Data Guide at https://rda.ucar.edu/datasets/ds628-1/, and the NCEP–NCAR dataset is obtained from NOAA PSL at https://psl.noaa.gov/data/gridded/data.ncep.reanalysis.html. CESM2 FC model output is available in the Earth System Grid Federation (ESGF) at http://esgf-node.llnl.gov/search/cmip6. CESM2 MD model output is available on the NCAR Climate Data Gateway website at https://www.earthsystemgrid.org/dataset/ucar.cgd.cesm2.mdpc.html. CESM2 NoENSO model output necessary to reproduce the figures in the paper is available at https://zenodo.org/uploads/10673083.

REFERENCES

Adam, O., T. Bischoff, and T. Schneider, 2016: Seasonal and interannual variations of the energy flux equator and ITCZ. Part I: Zonally averaged ITCZ position. *J. Climate*, **29**, 3219–3230, https://doi.org/10.1175/JCLI-D-15-0512.1.

——, and Coauthors, 2018: The TropD software package (v1): Standardized methods for calculating Tropical-width Diagnostics. *Geosci. Model Dev.*, **11**, 4339–4357, https://doi.org/10.5194/gmd-11-4339-2018.

Amaya, D. J., 2019: The Pacific Meridional Mode and ENSO: A review. *Curr. Climate Change Rep.*, **5**, 296–307, https://doi.org/10.1007/s40641-019-00142-x.

Bitz, C. M., K. M. Shell, P. R. Gent, D. A. Bailey, G. Danabasoglu, K. C. Armour, M. M. Holland, and J. T. Kiehl, 2012: Climate sensitivity of the Community Climate System Model, version 4. *J. Climate*, **25**, 3053–3070, https://doi.org/10.1175/JCLI-D-11-00290.1.

Caballero, R., 2007: Role of eddies in the interannual variability of Hadley cell strength. *Geophys. Res. Lett.*, **34**, L22705, https://doi.org/10.1029/2007GL030971.

Cai, W., B. Ng, G. Wang, A. Santoso, L. Wu, and K. Yang, 2022: Increased ENSO sea surface temperature variability under four IPCC emission scenarios. *Nat. Climate Change*, **12**, 228–231, https://doi.org/10.1038/s41558-022-01282-z.

Capotondi, A., and Coauthors, 2015: Understanding ENSO diversity. *Bull. Amer. Meteor. Soc.*, **96**, 921–938, https://doi.org/10.1175/BAMS-D-13-00117.1.

——, C. Deser, A. S. Phillips, Y. Okumura, and S. M. Larson, 2020: ENSO and Pacific Decadal Variability in the Community Earth System Model version 2. *J. Adv. Model. Earth Syst.*, **12**, e2019MS002022, https://doi.org/10.1029/2019MS002022.

Ceppi, P., and T. G. Shepherd, 2017: Contributions of climate feedbacks to changes in atmospheric circulation. *J. Climate*, **30**, 9097–9118, https://doi.org/10.1175/JCLI-D-17-0189.1.

——, Y.-T. Hwang, X. Liu, D. M. W. Frierson, and L. Hartmann, 2013: The relationship between the ITCZ and the Southern Hemispheric eddy-driven jet. *J. Geophys. Res. Atmos.*, **118**, 5136–5146, https://doi.org/10.1002/jgrd.50461.

Chemke, R., 2021: Future changes in the Hadley circulation: The role of ocean heat transport. *Geophys. Res. Lett.*, **48**, e2020GL091372, https://doi.org/10.1029/2020GL091372.

——, 2022: Large hemispheric differences in the Hadley cell strength variability due to ocean coupling. *npj Climate Atmos. Sci.*, **5**, 1, https://doi.org/10.1038/s41612-021-00225-3.

——, and L. M. Polvani, 2018: Ocean circulation reduces the Hadley cell response to increased greenhouse gases. *Geophys. Res. Lett.*, **45**, 9197–9205, https://doi.org/10.1029/2018GL079070.

——, and ——, 2019: Opposite tropical circulation trends in climate models and in reanalyses. *Nat. Geosci.*, **12**, 528–532, https://doi.org/10.1038/s41561-019-0383-x.

Chiang, J. C. H., and D. J. Vimont, 2004: Analogous Pacific and Atlantic meridional modes of tropical atmosphere–ocean variability. *J. Climate*, **17**, 4143–4158, https://doi.org/10.1175/JCLI4953.1.

Clement, A. C., 2006: The role of the ocean in the seasonal cycle of the Hadley circulation. *J. Atmos. Sci.*, **63**, 3351–3365, https://doi.org/10.1175/JAS3811.1.

Danabasoglu, G., and Coauthors, 2020: The Community Earth System Model Version 2 (CESM2). *J. Adv. Model. Earth Syst.*, **12**, e2019MS001916, https://doi.org/10.1029/2019MS001916.

Davis, N. A., and T. Birner, 2019: Eddy influences on the Hadley circulation. *J. Adv. Model. Earth Syst.*, **11**, 1563–1581, https://doi.org/10.1029/2018MS001554.

Deser, C., A. Phillips, V. Bourdette, and H. Teng, 2012: Uncertainty in climate change projections: The role of internal variability.

Climate Dyn., **38**, 527–546, https://doi.org/10.1007/s00382-010-0977-x.

Dima, I. M., and J. M. Wallace, 2003: On the seasonality of the Hadley cell. *J. Atmos. Sci.*, **60**, 1522–1527, https://doi.org/10.1175/1520-0469(2003)060<1522:OTSOTH>2.0.CO;2.

Feng, J., J. Li, F. Jin, Z. Liu, X. Nan, and Y. Guo, 2016: Contrasting responses of the Hadley circulation to equatorially asymmetric and symmetric meridional sea surface temperature structures. *J. Climate*, **29**, 8949–8963, https://doi.org/10.1175/JCLI-D-16-0171.1.

Feng, S., and Q. Fu, 2013: Expansion of global drylands under a warming climate. *Atmos. Chem. Phys.*, **13**, 10 081–10 094, https://doi.org/10.5194/acp-13-10081-2013.

Frierson, D. M. W., J. Lu, and G. Chen, 2007: Width of the Hadley cell in simple and comprehensive general circulation models. *Geophys. Res. Lett.*, **34**, L18804, https://doi.org/10.1029/2007GL031115.

——, and Coauthors, 2013: Contribution of ocean overturning circulation to tropical rainfall peak in the Northern Hemisphere. *Nat. Geosci.*, **6**, 940–944, https://doi.org/10.1038/ngeo1987.

Gastineau, G., H. L. Treut, and L. Li, 2008: Hadley circulation changes under global warming conditions indicated by coupled climate models. *Tellus*, **60A**, 863–884, https://doi.org/10.1111/j.1600-0870.2008.00344.x.

Hasan, M., S. Larson, and K. McMonigal, 2022: Hadley cell edge modulates the role of Ekman heat flux in a future climate. *Geophys. Res. Lett.*, **49**, e2022GL100401, https://doi.org/10.1029/2022GL100401.

Held, I. M., and A. Y. Hou, 1980: Nonlinear axially symmetric circulations in a nearly inviscid atmosphere. *J. Atmos. Sci.*, **37**, 515–533, https://doi.org/10.1175/1520-0469(1980)037<0515:NASCIA>2.0.CO;2.

——, and B. J. Hoskins, 1985: Large-Scale eddies and the general circulation of the troposphere. *Advances in Geophysics*, Vol. 28, Academic Press, 3–31, https://doi.org/10.1016/S0065-2687(08)60218-6.

——, and B. J. Soden, 2006: Robust responses of the hydrological cycle to global warming. *J. Climate*, **19**, 5686–5699, https://doi.org/10.1175/JCLI3990.1.

Hersbach, H., and Coauthors, 2020: The ERA5 global reanalysis. *Quart. J. Roy. Meteor. Soc.*, **146**, 1999–2049, https://doi.org/10.1002/qj.3803.

Holton, J. R., and G. J. Hakim, 2013: *An Introduction to Dynamic Meteorology*. Academic Press, 552 pp.

Hu, Y., H. Huang, and C. Zhou, 2018: Widening and weakening of the Hadley circulation under global warming. *Sci. Bull.*, **63**, 640–644, https://doi.org/10.1016/j.scib.2018.04.020.

Ji, X., J. Feng, J. Li, and X. Chen, 2023: Relationship between the Hadley circulation and tropical SST meridional structures under different thermal conditions in the Indo-Pacific warm pool. *Front. Mar. Sci.*, **9**, 1088276, https://doi.org/10.3389/fmars.2022.1088276.

Kalnay, E., and Coauthors, 1996: The NCEP/NCAR 40-year reanalysis project. *Bull. Amer. Meteor. Soc.*, **77**, 437–472, https://doi.org/10.1175/1520-0477(1996)077<0437:TNYRP>2.0.CO;2.

Kang, S. M., 2020: Extratropical influence on the tropical rainfall distribution. *Curr. Climate Change Rep.*, **6**, 24–36, https://doi.org/10.1007/s40641-020-00154-y.

——, and L. M. Polvani, 2011: The interannual relationship between the latitude of the eddy-driven jet and the edge of the Hadley cell. *J. Climate*, **24**, 563–568, https://doi.org/10.1175/2010JCLI4077.1.

——, I. M. Held, D. M. W. Frierson, and M. Zhao, 2008: The response of the ITCZ to extratropical thermal forcing: Idealized slab-ocean experiments with a GCM. *J. Climate*, **21**, 3521–3532, https://doi.org/10.1175/2007JCLI2146.1.

——, C. Deser, and L. M. Polvani, 2013: Uncertainty in climate change projections of the Hadley circulation: The role of internal variability. *J. Climate*, **26**, 7541–7554, https://doi.org/10.1175/JCLI-D-12-00788.1.

——, I. M. Held, and S.-P. Xie, 2014: Contrasting the tropical responses to zonally asymmetric extratropical and tropical thermal forcing. *Climate Dyn.*, **42**, 2033–2043, https://doi.org/10.1007/s00382-013-1863-0.

Kim, D., H. Kim, S. M. Kang, M. F. Stuecker, and T. M. Merlis, 2022: Weak Hadley cell intensity changes due to compensating effects of tropical and extratropical radiative forcing. *npj Climate Atmos. Sci.*, **5**, 61, https://doi.org/10.1038/s41612-022-00287-x.

Kim, H., S. M. Kang, J. E. Kay, and S.-P. Xie, 2022: Subtropical clouds key to Southern Ocean teleconnections to the tropical Pacific. *Proc. Natl. Acad. Sci. USA*, **119**, e2200514119, https://doi.org/10.1073/pnas.2200514119.

Kim, H.-K., and S. Lee, 2001: Hadley cell dynamics in a primitive equation model. Part II: Nonaxisymmetric flow. *J. Atmos. Sci.*, **58**, 2859–2871, https://doi.org/10.1175/1520-0469(2001)058<2859:HCDIAP>2.0.CO;2.

Kobayashi, S., and Coauthors, 2015: The JRA-55 reanalysis: General specifications and basic characteristics. *J. Meteor. Soc. Japan*, **93**, 5–48, https://doi.org/10.2151/jmsj.2015-001.

Larson, S. M., and B. P. Kirtman, 2015: Revisiting ENSO coupled instability theory and SST error growth in a fully coupled model. *J. Climate*, **28**, 4724–4742, https://doi.org/10.1175/JCLI-D-14-00731.1.

——, K. V. Pegion, and B. P. Kirtman, 2018: The South Pacific meridional mode as a thermally driven source of ENSO amplitude modulation and uncertainty. *J. Climate*, **31**, 5127–5145, https://doi.org/10.1175/JCLI-D-17-0722.1.

——, K. McMonigal, Y. Okumura, D. Amaya, A. Capotondi, K. Bellomo, I. R. Simpson, and A. C. Clement, 2024: Ocean complexity shapes sea surface temperature variability in a CESM2 coupled model hierarchy. *J. Climate*, **37**, 4931–4948, https://doi.org/10.1175/JCLI-D-23-0621.1.

Latif, M., and Coauthors, 2023: Strengthening atmospheric circulation and trade winds slowed tropical Pacific surface warming. *Commun. Earth Environ.*, **4**, 249, https://doi.org/10.1038/s43247-023-00912-4.

Lau, W. K. M., and K.-M. Kim, 2015: Robust Hadley circulation changes and increasing global dryness due to CO_2 warming from CMIP5 model projections. *Proc. Natl. Acad. Sci. USA*, **112**, 3630–3635, https://doi.org/10.1073/pnas.1418682112.

Levine, X. J., and T. Schneider, 2011: Response of the Hadley circulation to climate change in an aquaplanet GCM coupled to a simple representation of ocean heat transport. *J. Atmos. Sci.*, **68**, 769–783, https://doi.org/10.1175/2010JAS3553.1.

Li, Y., and Coauthors, 2023: Interannual variability of regional Hadley circulation and El Niño interaction. *Geophys. Res. Lett.*, **50**, e2022GL102016, https://doi.org/10.1029/2022GL102016.

Liu, G., Y.-O. Kwon, C. Frankignoul, and J. Lu, 2023: Understanding the drivers of Atlantic multidecadal variability using a stochastic model hierarchy. *J. Climate*, **36**, 1043–1058, https://doi.org/10.1175/JCLI-D-22-0309.1.

Lu, J., G. Chen, and D. M. W. Frierson, 2008: Response of the zonal mean atmospheric circulation to El Niño versus global

warming. *J. Climate*, **21**, 5835–5851, https://doi.org/10.1175/2008JCLI2200.1.

Luongo, M. T., N. G. Brizuela, I. Eisenman, and S.-P. Xie, 2024: Retaining short-term variability reduces mean state biases in wind stress overriding simulations. *J. Adv. Model. Earth Syst.*, **16**, e2023MS003665, https://doi.org/10.1029/2023MS003665.

McMonigal, K., and S. M. Larson, 2022: ENSO explains the link between Indian Ocean Dipole and meridional ocean heat transport. *Geophys. Res. Lett.*, **49**, e2021GL095796, https://doi.org/10.1029/2021GL095796.

——, S. Larson, S. Hu, and R. Kramer, 2023: Historical changes in wind-driven ocean circulation can accelerate global warming. *Geophys. Res. Lett.*, **50**, e2023GL102846, https://doi.org/10.1029/2023GL102846.

Mitas, C. M., and A. Clement, 2005: Has the Hadley cell been strengthening in recent decades? *Geophys. Res. Lett.*, **32**, L03809, https://doi.org/10.1029/2004GL021765.

——, and ——, 2006: Recent behavior of the Hadley cell and tropical thermodynamics in climate models and reanalyses. *Geophys. Res. Lett.*, **33**, L01810, https://doi.org/10.1029/2005GL024406.

Murphy, L. N., J. M. Klavans, A. C. Clement, and M. A. Cane, 2021: Investigating the roles of external forcing and ocean circulation on the Atlantic multidecadal SST variability in a large ensemble climate model hierarchy. *J. Climate*, **34**, 4835–4849, https://doi.org/10.1175/JCLI-D-20-0167.1.

Nguyen, H., A. Evans, C. Lucas, I. Smith, and B. Timbal, 2013: The Hadley circulation in reanalyses: Climatology, variability, and change. *J. Climate*, **26**, 3357–3376, https://doi.org/10.1175/JCLI-D-12-00224.1.

O'Gorman, P. A., 2011: The effective static stability experienced by eddies in a moist atmosphere. *J. Atmos. Sci.*, **68**, 75–90, https://doi.org/10.1175/2010JAS3537.1.

Oort, A. H., and J. J. Yienger, 1996: Observed interannual variability in the Hadley circulation and its connection to ENSO. *J. Climate*, **9**, 2751–2767, https://doi.org/10.1175/1520-0442(1996)009<2751:OIVITH>2.0.CO;2.

Pegion, K., C. M. Selman, S. Larson, J. C. Furtado, and E. J. Becker, 2020: The impact of the extratropics on ENSO diversity and predictability. *Climate Dyn.*, **54**, 4469–4484, https://doi.org/10.1007/s00382-020-05232-3.

Peixoto, J. P., and A. H. Oort, 1992: *Physics of Climate*. American Institute of Physics, 520 pp.

Peng, Q., S.-P. Xie, and C. Deser, 2024: Collapsed upwelling projected to weaken ENSO under sustained warming beyond the twenty-first century. *Nat. Climate Change*, **14**, 815–822, https://doi.org/10.1038/s41558-024-02061-8.

Pikovnik, M., Ž. Zaplotnik, L. Boljka, and N. Žagar, 2022: Metrics of the Hadley circulation strength and associated circulation trends. *Wea. Climate Dyn.*, **3**, 625–644, https://doi.org/10.5194/wcd-3-625-2022.

Quan, X.-W., H. F. Diaz, and M. P. Hoerling, 2004: Change in the tropical Hadley cell since 1950. *The Hadley Circulation: Present, Past and Future*, H. F. Diaz and R. S. Bradley, Eds., Advances in Global Change Research, Vol. 21, Springer, 85–120.

Robinson, W., 2006: Eddy-mediated interactions between low latitudes and the extratropics. *The Global Circulation of the Atmosphere*, T. Schneider and A. H. Sobel, Eds., Princeton University Press, 104–142.

Scheff, J., and D. M. W. Frierson, 2012: Robust future precipitation declines in CMIP5 largely reflect the poleward expansion of model subtropical dry zones. *Geophys. Res. Lett.*, **39**, L18704, https://doi.org/10.1029/2012GL052910.

Schmidt, D. F., and K. M. Grise, 2017: The response of local precipitation and sea level pressure to Hadley cell expansion. *Geophys. Res. Lett.*, **44**, 10 573–10 582, https://doi.org/10.1002/2017GL075380.

Schneider, E. K., and R. S. Lindzen, 1977: Axially symmetric steady-state models of the basic state for instability and climate studies. Part I. Linearized calculations. *J. Atmos. Sci.*, **34**, 263–279, https://doi.org/10.1175/1520-0469(1977)034<0263:ASSSMO>2.0.CO;2.

——, 1977: Axially symmetric steady-state models of the basic state for instability and climate studies. Part II. Nonlinear calculations. *J. Atmos. Sci.*, **34**, 280–296, https://doi.org/10.1175/1520-0469(1977)034<0280:ASSSMO>2.0.CO;2.

Schneider, T., and S. Bordoni, 2008: Eddy-mediated regime transitions in the seasonal cycle of a Hadley circulation and implications for monsoon dynamics. *J. Atmos. Sci.*, **65**, 915–934, https://doi.org/10.1175/2007JAS2415.1.

——, T. Bischoff, and G. H. Haug, 2014: Migrations and dynamics of the intertropical convergence zone. *Nature*, **513**, 45–53, https://doi.org/10.1038/nature13636.

Seager, R., N. Harnik, Y. Kushnir, W. Robinson, and J. Miller, 2003: Mechanisms of hemispherically symmetric climate variability. *J. Climate*, **16**, 2960–2978, https://doi.org/10.1175/1520-0442(2003)016<2960:MOHSCV>2.0.CO;2.

——, ——, W. A. Robinson, Y. Kushnir, M. Ting, H.-P. Huang, and J. Velez, 2005: Mechanisms of ENSO-forcing of hemispherically symmetric precipitation variability. *Quart. J. Roy. Meteor. Soc.*, **131**, 1501–1527, https://doi.org/10.1256/qj.04.96.

Seo, K.-H., S.-P. Yoon, J. Lu, Y. Hu, P. W. Staten, and D. M. W. Frierson, 2023: What controls the interannual variation of Hadley cell extent in the Northern Hemisphere: Physical mechanism and empirical model for edge variation. *npj Climate Atmos. Sci.*, **6**, 204, https://doi.org/10.1038/s41612-023-00533-w.

Shepherd, T. G., 2014: Atmospheric circulation as a source of uncertainty in climate change projections. *Nat. Geosci.*, **7**, 703–708, https://doi.org/10.1038/ngeo2253.

Shu, Q., Y. Zhang, D. J. Amaya, S. M. Larson, Y. Kosaka, J.-C. Yang, and X. Lin, 2023: Role of ocean advections during the evolution of the Pacific meridional modes. *J. Climate*, **36**, 4327–4343, https://doi.org/10.1175/JCLI-D-22-0296.1.

Stachnik, J. P., and C. Schumacher, 2011: A comparison of the Hadley circulation in modern reanalyses. *J. Geophys. Res.*, **116**, D22102, https://doi.org/10.1029/2011JD016677.

Sun, Y., L. Z. X. Li, G. Ramstein, T. Zhou, N. Tan, M. Kageyama, and S. Wang, 2019: Regional meridional cells governing the interannual variability of the Hadley circulation in boreal winter. *Climate Dyn.*, **52**, 831–853, https://doi.org/10.1007/s00382-018-4263-7.

Sutton, M., S. M. Larson, and E. Becker, 2024: New insights on ENSO teleconnection asymmetry and ENSO forced atmospheric circulation variability over North America. *Climate Dyn.*, **62**, 3189–3206, https://doi.org/10.1007/s00382-023-07058-1.

Tanaka, H. L., N. Ishizaki, and A. Kitoh, 2004: Trend and interannual variability of Walker, monsoon and Hadley circulations defined by velocity potential in the upper troposphere. *Tellus*, **56A**, 250–269, https://doi.org/10.3402/tellusa.v56i3.14410.

Vallis, G. K., 2017: *Atmospheric and Oceanic Fluid Dynamics*. Cambridge University Press, 965 pp.

——, P. Zurita-Gotor, C. Cairns, and J. Kidston, 2015: Response of the large-scale structure of the atmosphere to global

warming. *Quart. J. Roy. Meteor. Soc.*, **141**, 1479–1501, https://doi.org/10.1002/qj.2456.

Vecchi, G. A., and B. J. Soden, 2007: Global warming and the weakening of the tropical circulation. *J. Climate*, **20**, 4316–4340, https://doi.org/10.1175/JCLI4258.1.

Vimont, D. J., J. M. Wallace, and D. S. Battisti, 2003: The seasonal footprinting mechanism in the Pacific: Implications for ENSO. *J. Climate*, **16**, 2668–2675, https://doi.org/10.1175/1520-0442(2003)016<2668:TSFMIT>2.0.CO;2.

Voigt, A., and T. A. Shaw, 2015: Circulation response to warming shaped by radiative changes of clouds and water vapour. *Nat. Geosci.*, **8**, 102–106, https://doi.org/10.1038/ngeo2345.

Walker, C. C., and T. Schneider, 2005: Response of idealized Hadley circulations to seasonally varying heating. *Geophys. Res. Lett.*, **32**, L06813, https://doi.org/10.1029/2004GL022304.

——, and ——, 2006: Eddy influences on Hadley circulations: Simulations with an idealized GCM. *J. Atmos. Sci.*, **63**, 3333–3350, https://doi.org/10.1175/JAS3821.1.

Watt-Meyer, O., and D. M. W. Frierson, 2019: ITCZ width controls on Hadley cell extent and eddy-driven jet position and their response to warming. *J. Climate*, **32**, 1151–1166, https://doi.org/10.1175/JCLI-D-18-0434.1.

Wettstein, J. J., and J. M. Wallace, 2010: Observed patterns of month-to-month storm-track variability and their relationship to the background flow. *J. Atmos. Sci.*, **67**, 1420–1437, https://doi.org/10.1175/2009JAS3194.1.

Willison, J., W. A. Robinson, and G. M. Lackmann, 2015: North Atlantic storm-track sensitivity to warming increases with model resolution. *J. Climate*, **28**, 4513–4524, https://doi.org/10.1175/JCLI-D-14-00715.1.

Xia, Y., Y. Hu, and J. Liu, 2020: Comparison of trends in the Hadley circulation between CMIP6 and CMIP5. *Sci. Bull.*, **65**, 1667–1674, https://doi.org/10.1016/j.scib.2020.06.011.

Yun, K.-S., J.-Y. Lee, A. Timmermann, K. Stein, M. F. Stuecker, J. C. Fyfe, and E.-S. Chung, 2021: Increasing ENSO–rainfall variability due to changes in future tropical temperature–rainfall relationship. *Commun. Earth Environ.*, **2**, 43, https://doi.org/10.1038/s43247-021-00108-8.

Yuval, J., and Y. Kaspi, 2020: Eddy activity response to global warming–like temperature changes. *J. Climate*, **33**, 1381–1404, https://doi.org/10.1175/JCLI-D-19-0190.1.

Zaplotnik, Ž., M. Pikovnik, and L. Boljka, 2022: Recent Hadley circulation strengthening: A trend or multidecadal variability? *J. Climate*, **35**, 4157–4176, https://doi.org/10.1175/JCLI-D-21-0204.1.

Zhang, H., A. Clement, and P. D. Nezio, 2014: The South Pacific meridional mode: A mechanism for ENSO-like variability. *J. Climate*, **27**, 769–783, https://doi.org/10.1175/JCLI-D-13-00082.1.

Zhou, C., J. Lu, Y. Hu, and M. D. Zelinka, 2020: Responses of the Hadley circulation to regional sea surface temperature changes. *J. Climate*, **33**, 429–441, https://doi.org/10.1175/JCLI-D-19-0315.1.

Zurita-Gotor, P., and P. Álvarez-Zapatero, 2018: Coupled interannual variability of the Hadley and Ferrel cells. *J. Climate*, **31**, 4757–4773, https://doi.org/10.1175/JCLI-D-17-0752.1.